PoS(FPCP2016)003

Experimental Overview of ϕ_3

Ian J. Watson[*][†]

University of Tokyo

E-mail: ian.watson@hep.phys.s.u-tokyo.ac.jp

The CKM angle ϕ_3 (also known as γ) is currently the least-constrained of the Unitary Triangle angles, but can be determined to sub-degree precision in $B \to DK$ decay without theoretical uncertainty in the Standard Model. This makes it an attractive Standard Model reference measurement. We present an overview of recent measurements of ϕ_3 related decay modes from LHCb, Belle and BaBar and discuss prospects for future measurements.

---

[*]Speaker.

[†]On behalf of the Belle Collaboration.

1. Introduction

In the Standard Model (SM) of particle physics, the only source of CP-violation comes from an irreducible complex phase in the 3×3 Cabibbo-Kobayashi-Maskawa (CKM) matrix V which describes quark-flavor mixing in weak interactions [1, 2]. The unitarity of the mixing matrix imposes relations on the elements of V, including $V_{ud}V_{ub}^* + V_{cd}V_{cb}^* + V_{td}V_{tb}^* = 0$, which defines a triangle on the complex plane. Many measurements of SM particle decays, particularly B mesons, can be interpreted as constraints on the length of the sides and angles of this triangle.

$\phi_3 = \arg\left(-\frac{V_{ud}V_{ub}^*}{V_{cd}V_{cb}^*}\right)$ is currently the least constrained of the Unitary Triangle angles. It is, however, measurable with tree level $b \to u$ and $b \to c$ interference with negligible loop contribution that results in theory uncertainties of only $O(10^{-7})$. Therefore, with large datasets, there is potential to measure ϕ_3 at or below $1°$, compared with the current uncertainty of about $8°$ (as will be discussed later).

Three experiments are mainly responsible for the current measurements of ϕ_3. These are the B-factories Belle and Babar, and the LHCb forward-spectrometer on the LHC. Belle is a hermetic detector on KEKB asymmetric e^+e^- collider [3]. It started in 1999 with data taken until 2010. A total of 772×10^6 $\Upsilon(4S) \to B\bar{B}$ events were collected over the course of its lifetime. Babar is a hermetic detector which operated on the SLAC PEP-II asymmetric e^+e^- collider [4]. It operated from 1999 until 2008 collecting $467 \pm 5 \times 10^6$ $\Upsilon(4S) \to B\bar{B}$ events. LHCb exploits the large forward $pp \to b\bar{b}X$ cross section in multi-TeV collisions. The detector is optimised for flavour physics with dedicated triggers, precision vertexing and excellent particle identification capabilities. LHCb has reported results from 1 fb^{-1} of data taken in 2011 at 7 TeV and 2 fb^{-1} of data taken in 2012 at 8 TeV [5].
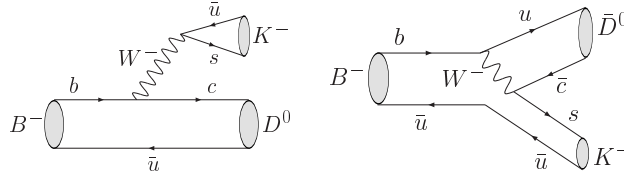
Figure 1: Example Feynman diagrams for $B^\pm \to DK^\pm$.

Experimentally, $B \to D^{(*)}K^{(*)}$, where the D decays in a channel common to D^0 & $\bar{D}^0$, provides the tree level $b \to u$ and $b \to c$ interference. This is illustrated in figure 1 showing Feynman diagrams for the processes involved in the $B^- \to DK^-$. The amplitude for the decay can be written as

$$A(B^- \to DK^-) \propto A_{D^0} + r_B e^{i(\delta_B \pm \phi_3)} A_{\bar{D}^0}, \tag{1.1}$$

where δ_B is the relative strong phase between the B decay amplitudes and r_B is the ratio between the amplitudes $r_B = \frac{|A(B^- \to \bar{D}^0 K^-|)}{|A(B^- \to D^0 K^-)|} \approx \frac{|V_{cs}V_{ub}^*|}{|V_{us}V_{cb}^*|} f_{col} \approx 0.1$ for $B^\pm \to DK^\pm$ (for $B^\pm \to D\pi^\pm$ $r_B \approx 0.01$), where $f_{col} \approx \frac{1}{3}$ is a colour suppression factor. Current measurements are statistically limited by the small B and D branching fractions and the limited interference due to the size of r_B. Expanding out the D decay amplitude and squaring the amplitude, the expression for the partial width can be written as

$$\Gamma(B^\pm \to DK^\pm) \propto r_D^2 + r_B^2 + 2r_B r_D \cos(\delta_B + \delta_D \mp \phi_3), \tag{1.2}$$

1

where r_D is the ratio between the D^0 and $\bar{D}^0$ decay mode amplitudes, and δ_D their relative phase.

Several methods of measurement have been proposed which are typically classified based on the way the D decays. These main areas are: analyses where the D decays to CP eigenstates (GLW), decay modes involving doubly-Cabibbo suppressed (DCS) decays of the Cabibbo-favored D, e.g. $D \to K^+\pi^-$ (ADS), and Dalitz analysis of 3-body decays (GGSZ). We will report on the results of these analyses in turn, and follow with a discussion of the combination of the information into a final constraint on ϕ_3. We will also briefly discuss the outlook for future measurements.

2. Methods

2.1 GLW

The GLW method [6, 7] uses D decay modes to CP eigenstates. These are denoted D_+ (D_-) for CP-even (odd) decay. In equation 1.2 this gives the constraints that $r_D = 1$ and $\delta_D = 0(\pi)$ for CP-even (-odd) decays. This leads to the following observables used in the analysis of GLW modes:

$$R_{CP\pm} = \frac{\Gamma(B^+ \to D^0_\pm K^+) + \Gamma(B^- \to D^0_\pm K^-)}{\Gamma(B^- \to D^0 K^-) + \Gamma(B^+ \to \bar{D}^0 K^+)} = 1 + r_B^2 \pm 2r_B \cos\phi_3 \cos\delta_B$$

$$A_{CP\pm} = \frac{\Gamma(B^+ \to D^0_\pm K^+) - \Gamma(B^- \to D^0_\pm K^-)}{\Gamma(B^+ \to D^0_\pm K^+) + \Gamma(B^- \to D^0_\pm K^-)} = \frac{\pm 2r_B \sin\phi_3 \sin\delta_B}{R_{CP\pm}},$$

where $\Gamma(B^- \to D^0 K^-)$ and $\Gamma(B^- \to D^0 K^-)$ are the total rates of the decays of the D^0 to known flavor states, which can be measured in conjunction with the CP modes.

CP-even decays that have been used include $D \to K^+K^-$, $D \to \pi^+\pi^-$; CP-odd decays include $D \to K_S\pi^0$, $D \to K_S\omega$ ($D \to K_S\phi$ is excluded due to its use in the GGSZ $D \to K_S K^+K^-$ analysis). In general, the modes used in GLW analyses have a larger rate but lower observable interference than the ADS method.
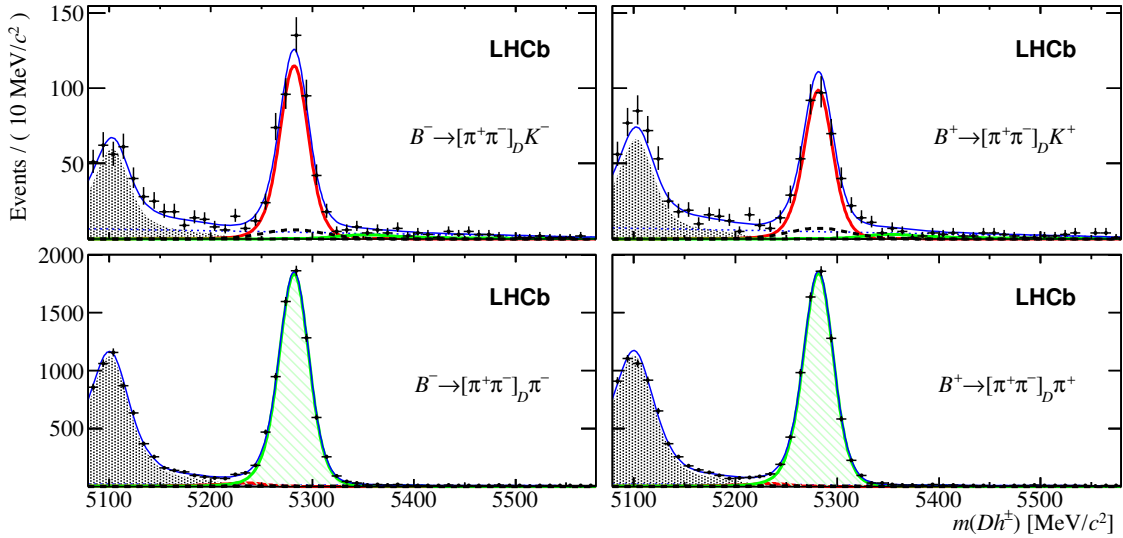
Figure 2: B mass spectrum for the GLW mode $B^\pm \to DK^\pm$, $D \to \pi^+\pi^-$ from the LHCb GLW analysis.

LHCb have recently released a complete analysis of their 7 and 8 TeV datasets, which includes the GLW modes [8]. They use a BDT for background suppression, fit in mass and share aspects of PDF across fits. This includes constraining cross-feed ($D\pi$ in DK) using known particle identification efficiencies and fixing the charmless cross-feed relative to the favored $B \to D\pi$, as well, the partially reconstructed backgrounds are modelled. Figure 2 shows the B mass spectrum for one mode.

The results are $A_{CP}^{\pi\pi} = 0.128 \pm 0.037 \pm 0.012$ and $R_{CP}^{\pi\pi} = 1.002 \pm 0.040 \pm 0.026 \pm 0.010$, where the final uncertainty is from the assumption $r_B^{D\pi} = 0$.
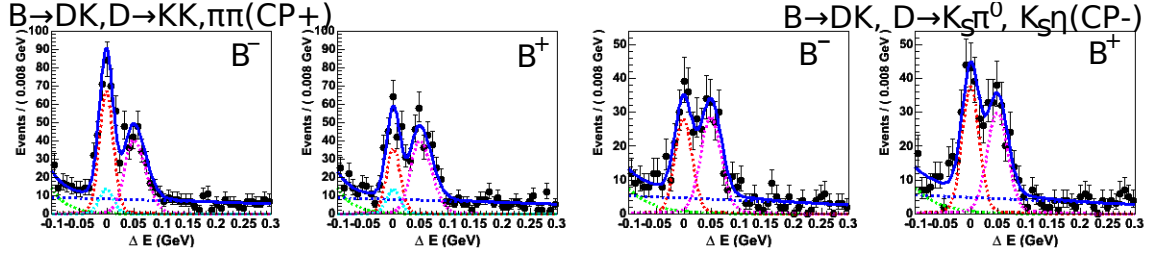
Figure 3: *CP* even (left) and *CP* odd (right) $\Delta E = E_{DK} - E_{beam}$ distributions for the GLW analysis of the Belle collaboration. Shown are fit components for the signal $B \to DK$, the cross-feed $B \to D\pi$, and the overall fit.

B factories still have the advantage in *CP*-odd states where neutral π^0/η reconstruction becomes necessary. An example is shown in figure 3 of the Belle GLW analysis, presented at Lepton-Photon 2011. The final results are: $R_{CP-} = 1.13 \pm 0.09 \pm 0.05$, $A_{CP-} = -0.12 \pm 0.06 \pm 0.01$ and $R_{CP+} = 1.03 \pm 0.07 \pm 0.02$, $A_{CP+} = +0.29 \pm 0.06 \pm 0.02$. The $A_{CP\pm}$ shows expected sign change between the *CP*-odd and *CP*-even states.

The HFAG collaboration has created a combination of ϕ_3 results for 2016, this is shown in figure 4 [9]. Using the combination the results and the equations presented giving the ratxoe of interference above, an estimate for the underlying physics parameters r_B, ϕ_3 and δ_B can be obtained. There is, however, an eight-fold degeneracy in extraction of ϕ_3 through use of the GLW method.

2.2 ADS Modes

The ADS [10, 11] method proceeds by choosing modes with interference through the favored and doubly-Cabibbo-suppressed decays of the D. The favored D decay follows a suppressed decay of the B meson, while the suppressed D decay follows favored B decay. The suppression factors for the D and B are roughly similar, leading to relatively similar amplitudes for either decay path. Therefore, the possible *CP* asymmetry is enhanced, though only modes where the overall branching fraction is small (due all the decay paths being suppressed) can be used.
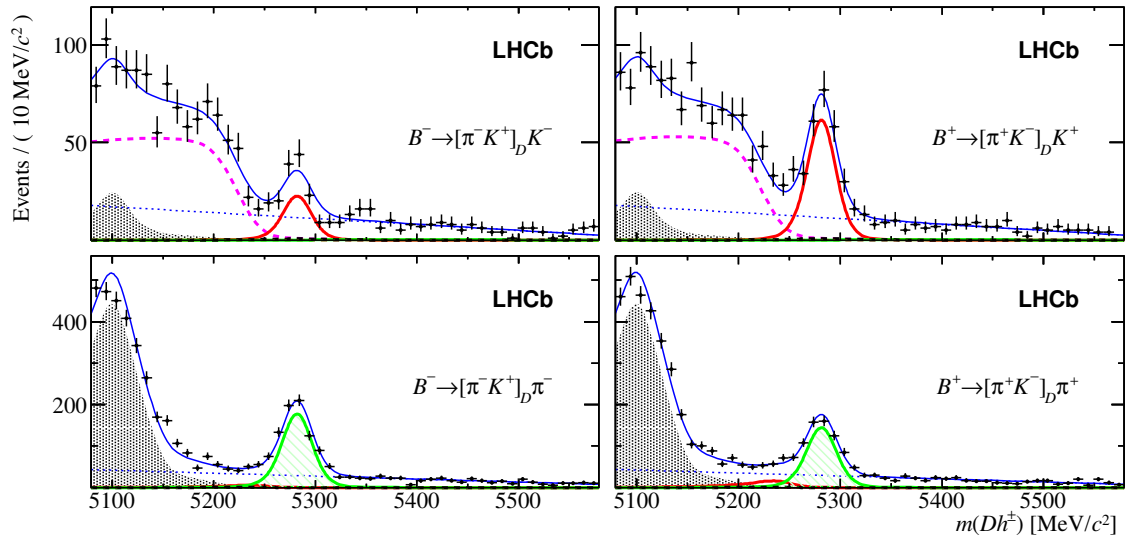
Observables (using $D \to K\pi$ as an example) that are used when analysing ADS modes are:

$$R_{ADS} = \frac{\Gamma(B^+ \to [K^-\pi^+]_D K^+) + \Gamma(B^- \to [K^+\pi^-]_D K^-)}{\Gamma(B^+ \to [K^+\pi^-]_D K^+) + \Gamma(B^- \to [K^-\pi^+]_D K^-)} = r_B^2 + r_D^2 + 2r_B r_D \cos(\delta_B + \delta_D) \cos\phi_3$$

$$A_{ADS} = \frac{\Gamma(B^+ \to [K^-\pi^+]_D K^+) - \Gamma(B^- \to [K^+\pi^-]_D K^-)}{\Gamma(B^+ \to [K^-\pi^+]_D K^+) + \Gamma(B^- \to [K^+\pi^-]_D K^-)} = \frac{2r_B r_D R \sin(\delta_B + \delta_D) \sin\phi_3}{R_{ADS}},$$
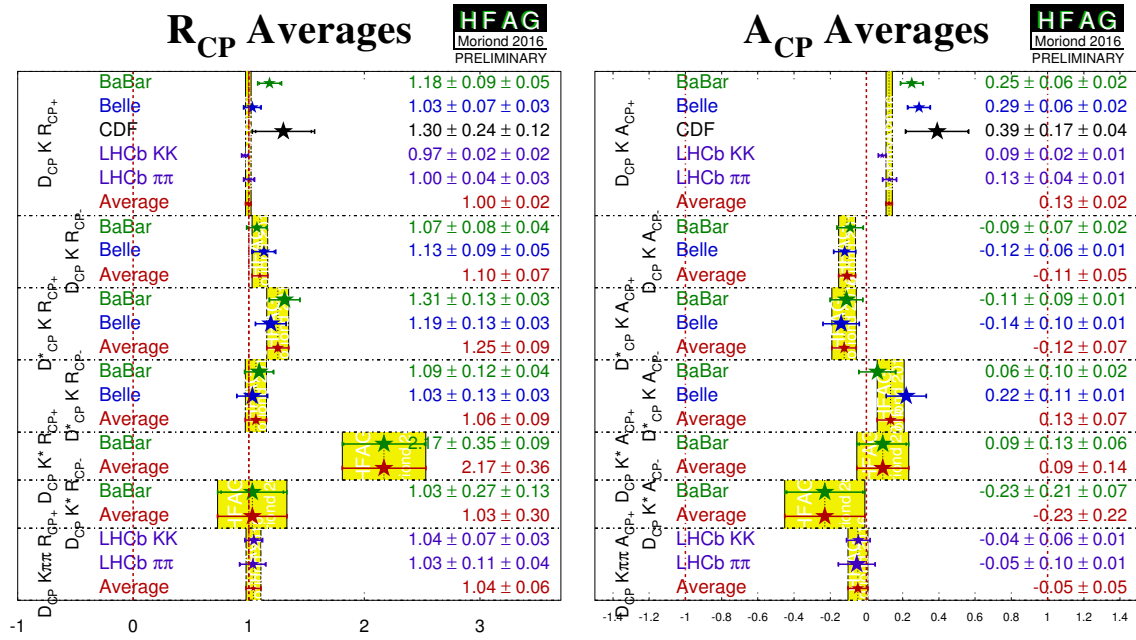
Figure 4: HFAG combination of GLW results [9]. The figures present the HFAG 2016 combination along with the inputs used from Belle, Babar, LHCb and CDF.

Figure 5: B mass distributions from the LHCb analysis of the ADS mode $B^{\pm} \to [\pi K]_D K^{\pm}$.

4

where $r_D = \left| \frac{A(D^0 \rightarrow K^+ \pi^-)}{A(D^0 \rightarrow K^- \pi^+)} \right|$, and δ_D can be obtained directly.

An example LHCb ADS analysis, of $B^\pm \rightarrow [\pi K]_D K^\pm$, is shown in figure 5. As for the GLW analysis, which is reported in the same paper [8], BDT background suppression and shared PDF parameters are used. The results are $A_{ADS}^{\pi K} = -0.403 \pm 0.056 \pm 0.011$, $R_{ADS}^{\pi K} = 0.0188 \pm 0.0011 \pm 0.0010$, which gives 8σ evidence for *CP*-violation in $B^\pm \rightarrow [\pi^\pm K^\mp]K^\pm$.
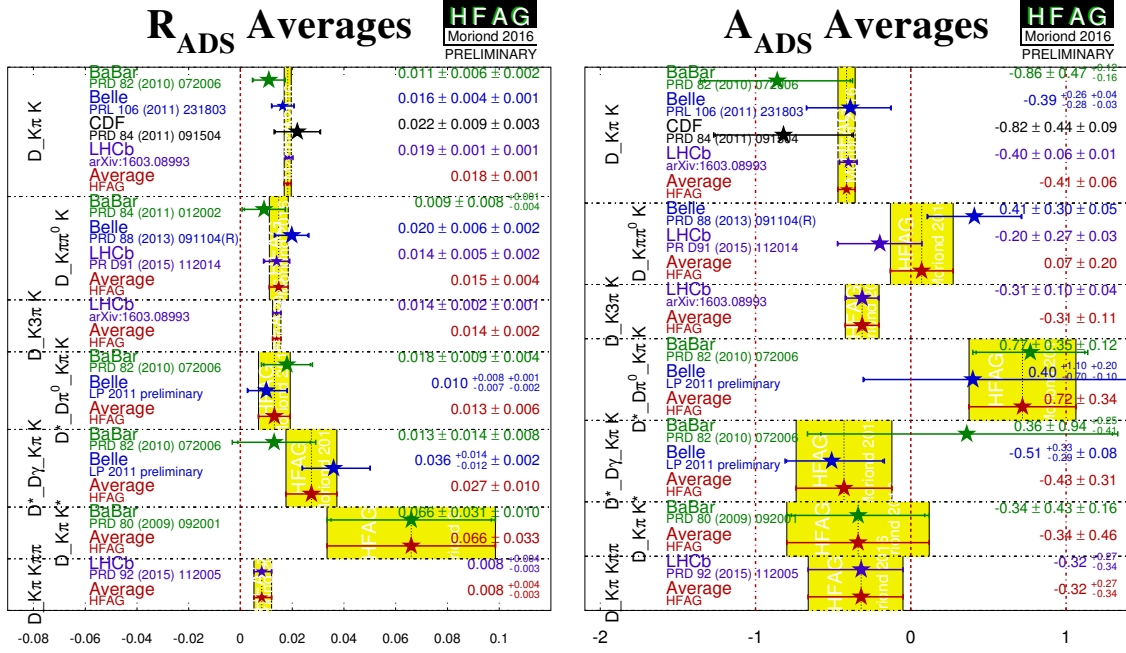
Figure 6: The ADS Combination (HFAG Moriond 2016 Preliminary) The figures shows the HFAG Combination against inputs from Belle, Babar, LHCb, CDF.

The HFAG 2016 combination for ADS modes is shown in figure 6 [9].

2.3 4-body final states
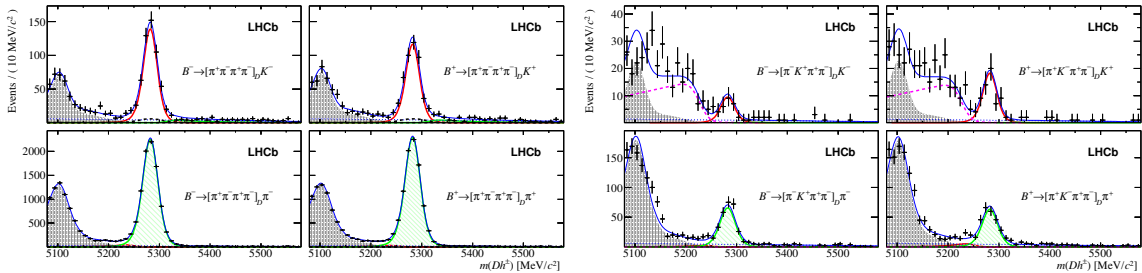
Figure 7: Mass distributions from the LHCb analyses of the 4-body decay modes $D \rightarrow \pi^+ \pi^- \pi^+ \pi^-$ and $D \rightarrow K^- \pi^+ \pi^+ \pi^-$.

The GLW and ADS analyses can both be extended to the case of four-body decays. LHCb calls these "quasi"-GLW and -ADS analyses and released them in conjunction with the ADS and

GLW analyses [8]. They studied the 4-body decay modes $D \to \pi^+\pi^-\pi^+\pi^-$ and $D \to K^-\pi^+\pi^+\pi^-$. The distributions for these decays are shown in figure 7.

For the GLW-like $D \to \pi^+\pi^-\pi^+\pi^-$, interference is reduced by measured CP-even fraction of states $F_+^{4\pi} = 0.737 \pm 0.028$ measured in CLEO data [12]. This factor enters as $2F_+^{4\pi} - 1$ multiplied into the usual GLW A_{CP+}, R_{CP+} equations. The results here are $A^{4\pi} = 0.10 \pm 0.03 \pm 0.02$, $R^{4\pi} = 0.97 \pm 0.04 \pm 0.02$, 2.7σ CP violation effect.

In $D \to K^-\pi^+\pi^+\pi^-$, the sensitivity to ϕ_3 is reduced by coherence factor $\kappa^{K3\pi} = 0.32 \pm 0.10$ and requires knowledge of the averaged strong-phase difference $\delta^{K3\pi}$ which has been measured in a CLEO and LHCb combined analysis [13]. The equations are modified in this case to $R_{ADS} = r_B^2 + r_D^2 + 2r_B r_D \kappa_D^{K3\pi} \cos(\delta_B + \delta_D^{K3\pi} - \gamma)$. LHCb finds the results $A^{\pi K\pi\pi} = -0.313 \pm 0.102 \pm 0.038$, $R^{\pi K\pi\pi} = 0.0140 \pm 0.0015 \pm 0.0006$.

As for the GLW and ADS analyses, these measurements are ultimately used in a combination to find the underlying physics parameters, including ϕ_3, governing these decays.

2.4 GGSZ
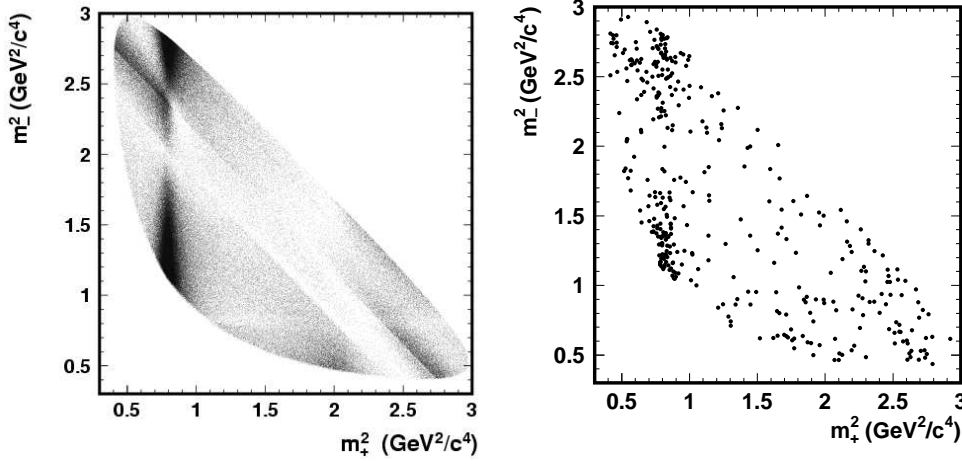
Figure 8: Dalitz plots of reconstructed data from $D^\pm \to \pi D$ (left [14]) and $B \to DK$ decays (right [15]) with $D \to K_S \pi^+\pi^-$ from Belle.

The GGSZ method uses the three-body decays of the D, $K_S h^+ h^-$ where $h = \pi^\pm, K^\pm$. In the following we will ignore mixing and CP-violation in the D system, as the effect of this is currently smaller than the uncertainties from the analyses. Further, as precision increases, it is straightforward to account for it when interpreting the measurements. The decay amplitude of equation 1.1 is then a function of the D kinematics, which can be expressed in terms of the Dalitz plot variables. Letting $(m_+^2, m_-^2) = (M(K_S h^+)^2, M(K_S h^-)^2)$, the partial-width for B^- may then be written as

$$\Gamma_{B^-}(m_+^2, m_-^2) \propto |A_D|^2 + r_B^2 |A_{\bar{D}}|^2 + 2\left(x_\pm \Re(A_D A_{\bar{D}}^*) + y_\pm \Im(A_{\bar{D}} A_D^*)\right), \qquad (2.1)$$

where we introduced, separately for B^+ and B^-, $(x_\pm, y_\pm) = r_B(\cos(\pm\phi_3 + \delta_B), \sin(\pm\phi_3 + \delta_B))$, a Cartesian reinterpretation of the interference parameters, which are used as the physical bound at $r_B = 0$ introduces a bias when directly fitting r_B. The rate for B^+ is given by the equation with

$A_{\bar{D}} \leftrightarrow A_D$. When plotted on the (x,y) plane, the two (x,y) are constrained to fall on the same circle of radius r_B, and their opening angle is twice ϕ_3. Thus, if we know the amplitude of the flavor-state Dalitz plot we can measure ϕ_3 by analysing the $D - \bar{D}$ interference using the D Dalitz plots in $B^{\pm} \rightarrow DK^{\pm}$ [18, 19].

The analyses start by using the flavour decays to fix A_D. For example, in the decay $D^{*\pm} \rightarrow \pi^{\pm}D$ the D is in a fixed flavor state based on the charge of the pion, so a Dalitz analysis of this mode can be used to find the D decay amplitude. Then, this fixed amplitude is used as input into an analysis of the $B^{\pm} \rightarrow DK^{\pm}$ D Dalitz, which separately measures the interference in terms of (x,y) for B^+ and B^-. The two measurements can be combined to give a measurement of ϕ_3, but, as for the other modes, this is usually done in the context of a combined fit to all $B \rightarrow DK$ measurements.

Initial analyses followed this procedure of constructing a Dalitz amplitude model which was fit in the $D^{*\pm}$ mode. Fitting the Dalitz amplitude, however, leads to a model-dependent uncertainty. The systematic uncertainty is derived by changing the parameters of the amplitude model, including additional resonances in the model for example, and quoting the resultant shift as a systematic uncertainty. For example, the Belle final analysis using this technique quoted the ϕ_3 systematic uncertainty due to model-dependence as $\sigma_{\phi_3} = 8.9°$ [15]. This, however, is a rather *ad hoc* measure, and so new methods with quantifiable and reducible uncertainties were searched for.
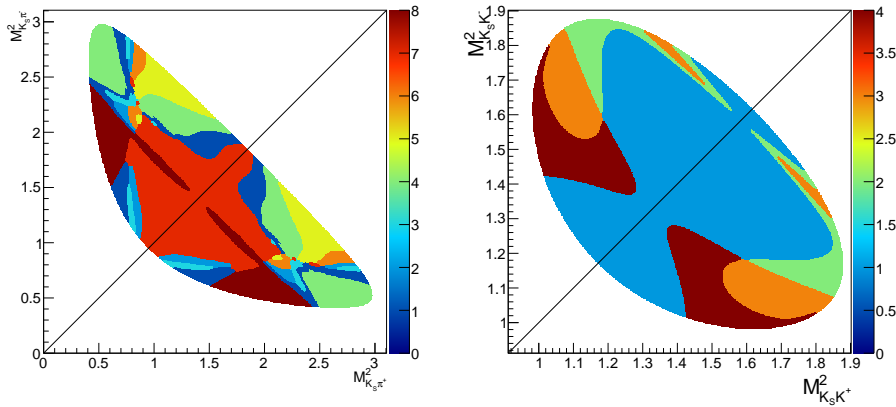
Figure 9: Examples of Dalitz binnings used in the model independent GGSZ analysis of $B \rightarrow DK$. Shown are the "Optimal" $K_S \pi^+ \pi^-$ binning (left) and 4 bins equal $\Delta \delta_D$ $K_S K^+ K^-$ (right).

A different approach using a binned Dalitz plot has been developed, which eliminates the need to fit a model of the Dalitz amplitude. In the model-independent method one the Dalitz plot is divided into 2N bins, labeled $i \in -N, .., -1, 1, .., N$, with the $-i^{th}$ bin equivalent to the ith bin but with the Dalitz variables exchanged $m^2_+ \leftrightarrow m^2_-$. Once the Dalitz plot has been binned, the number of events expected in a bin is proportional to the integral of the partial-width over the phase-space d of the bin. In the case of $D^{*\pm} \rightarrow D\pi^{\pm}$, this means the number of events reconstructed in a bin K_i is proportional to the integral over the amplitude $|A_D|^2$, while K_{-i} is proportional to the integral over $|A_{\bar{D}}|^2$ given the assumption of *CP*-invariance. For $B^- \rightarrow DK^-$ the number of events in a bin N_i can then be expressed as

$$N_i \propto K_i + r^2_{\pm} K_{-i} + 2\sqrt{K_i K_{-i}} (x_{\pm} c_i + y_{\pm} s_i) \tag{2.2}$$

where we have used the number of flavor tagged events in a given bin K_i and where we introduce the averaged phase variation over a Dalitz bin $\mathscr{D}_i$

$$(s_i, c_i) = (-s_{-i}, c_{-i}) \equiv \left(\frac{\int_{\mathscr{D}_i} |A_D^{+-}||A_D^{-+}| \sin \Delta \delta_D^{+-} d\mathscr{D}}{\sqrt{\int_{\mathscr{D}_i} |A_D^{+-}| d\mathscr{D} \int_{\mathscr{D}_i} |A_D^{-+}| d\mathscr{D}}}, \frac{\int_{\mathscr{D}_i} |A_D^{+-}||A_D^{-+}| \cos \Delta \delta_D^{+-} d\mathscr{D}}{\sqrt{\int_{\mathscr{D}_i} |A_D^{+-}| d\mathscr{D} \int_{\mathscr{D}_i} |A_D^{-+}| d\mathscr{D}}} \right) \quad (2.3)$$

These values can be measured from quantum correlated $D\bar{D}$ decays of $\psi(3770)$, as has been done at CLEO [20]. The binnings measured at CLEO were set to minimize expected phase variation over bins for $K_S K^+ K^-$ or optimize sensitivity to ϕ_3 in the case of $K_S \pi^+ \pi^-$. These binnings are shown in figure 9. Finally, note that while the binnings are set based on optimizations using model-dependent results, the results obtained in the model-independent method are not biased by the binning. A poor choice in binning reduces the statistical sensitivity of the method by reducing the amplitudes of the values of c_i and s_i, which, from equation 2.2, are measures of the sensitivity of the method.
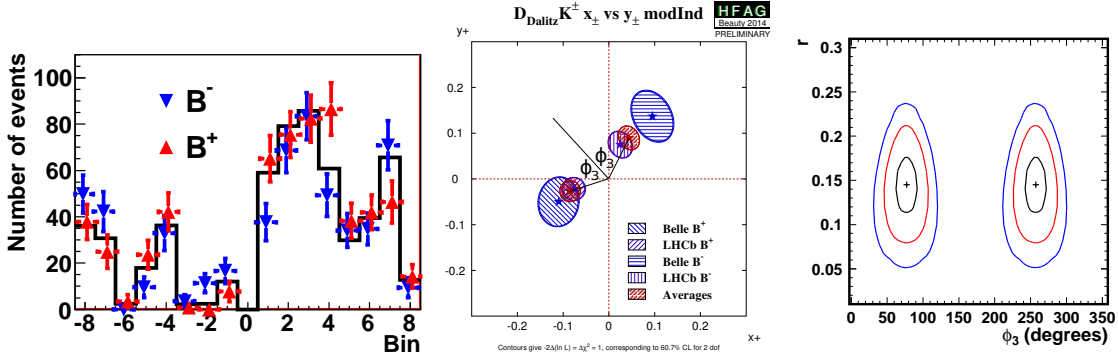
Figure 10: Results for the model independent analysis from Belle [21]. The results from Belle for (left) $[K_S \pi^+ \pi^-]_D$ for N signal in bins compared with the number of events expected from the D flavor-decay Dalitz, then (middle) the fit in $(x_\pm, y_\pm)$ plane (including comparisons with the LHCb results [22] and the HFAG combination [9]), and (right) converted to constraints in the (r_B, ϕ_3).

The results of the first model-independent analysis, which was performed by the Belle collaboration [21], are shown in figure 10. In terms of the underlying physics parameters, the Belle model-dependent analysis found $\phi_3 = (80.8^{+13.1}_{-14.8} \pm 5.0 \pm 8.9)^\circ$ where the quoted uncertainties are statistical, systematic, and the uncertainty due to model-dependency. The model independent analysis finds $\phi_3 = (77.3^{+15.1}_{-14.9} \pm 4.1 \pm 4.3)^\circ$ where the uncertainties are now statistical, systematic, and the uncertainty due to the CLEO uncertainty on (c_i, s_i). Note that the model-independent analysis uses 710 fb^{-1}, whereas 605 fb^{-1} is used for the Dalitz analysis. The model independent analysis also measures $r_B = 0.145 \pm 0.03 \pm 0.01 \pm 0.01$, whereas the Dalitz analysis gives $r_B = 0.16 \pm 0.04 \pm 0.01^{+0.05}_{-0.01}$, and this smaller value directly translates into a higher uncertainty on ϕ_3.

LHCb [22] has performed a model-independent analysis which includes both $K_S \pi^+ \pi^-$ and $K_S K^+ K^-$ for the D decay. Using a frequentist Neyman construction with Feldman-Cousins ordering, they interpret this as constraints on the underlying physics parameters $\phi_3 = (62^{+15}_{-14})^\circ$, $r_B = 0.080^{+0.019}_{-0.021}$.
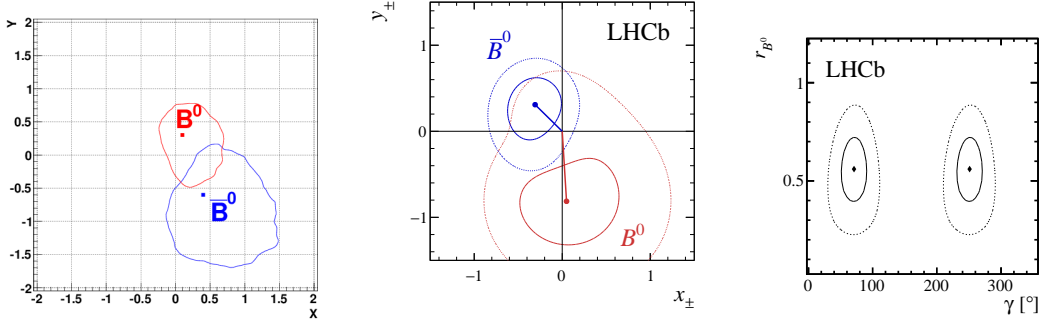
Figure 11: Belle (left) and LHCb (middle) results for $B^0 \to DK^{*0}$. The fitted (x,y) for B^0 is shown in red, and $\bar{B}^0$ is shown in blue. For LHCb, these results are translated into confidence volumes in $(\phi_3, r_{B^0}, \delta_{B^0})$ and are here shown projected on the (ϕ_3, r_{B^0}) plane (right) for 68.3% (solid) and 95.5% (dotted) confidence levels when projected onto one-dimension.

The model independent method has also been used for $B^0 \to DK^{*0}$, $K^{*0} \to K^+\pi^-$. This mode is amenable to the GGSZ method as the B^0 flavor is tagged by the kaon charge. The GGSZ equation 2.2 must be slightly modified to $N_i^{\pm} \propto K_i + r_{B^0}^2 K_{-i} + 2\kappa\sqrt{K_i K_{-i}}(xc_i + ys_i)$, where $\kappa \approx 0.958$, a coherence factor for the chosen $K^+\pi^-$ region, has been measured by LHCb [23]. Results, in terms of the fitted parameters x and y, are shown in figure 11. Belle sets an upper limit of $r_S < 0.87$ (68%CL) [16]. Their results for B^+ are $(x,y) = (0.05 \pm 0.35 \pm 0.02, 0.81 \pm 0.28 \pm 0.06)$, and for B^- they measure $(x,y) = (0.31 \pm 0.20 \pm 0.04, 0.31 \pm 0.21 \pm 0.05)$. As before, LHCb translates this into constraints on the physics parameters $r_S = 0.56 \pm 0.17$, $\phi_3 = (71 \pm 20)°$ [17]. LHCb also has model-dependent Dalitz with consistent fit results.
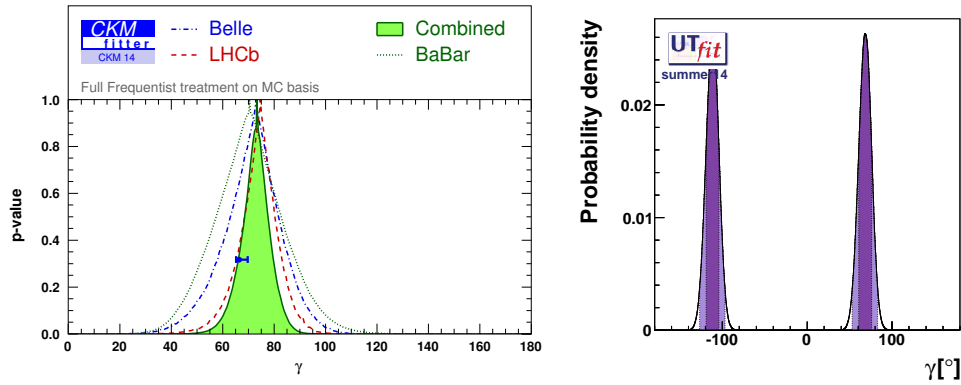
2.5 Combination
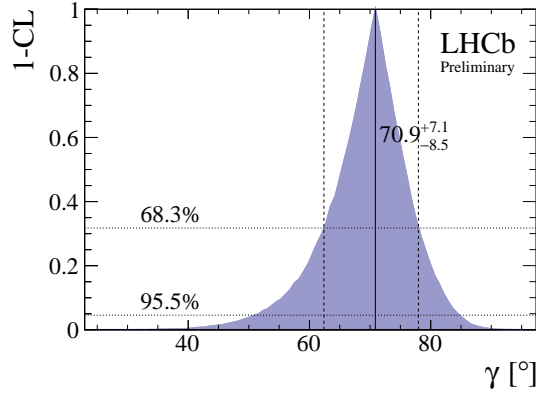
Figure 12: The ϕ_3 1-CL distribution from the LHCb 2016 combination [24].

Using the plugin method, LHCb has produced an LHCb-only average for ϕ_3. They include their latest 2016 results [24]. The result is shown in figure 12. They find $\phi_3 = (70.9^{+7.1}_{-8.5})°$.

Two groups, CKMFitter [25] and UTFit [26], have produced world-averages of ϕ_3 and the related decay parameters including all experimental results as of 2014. A combination of all ex-

Figure 13: Combinations of ϕ_3 measurements from the CKMFitter (left) and UTFit (right) collaborations. The combinations both include results up to 2014.

periments with the latest data is yet to be produced. They also produce predictions for ϕ_3, based on CKM measurements excluding direct ϕ_3 and assuming SM physics.

The CKMFitter group uses a frequentist framework to interpret the experimental data. They find $\phi_3 = (73.2^{+6.3}_{-7.0})°$. This can be compared with, and is compatible with their CKM prediction of $\phi_3 = (66.9^{+1.0}_{-3.7})°$. The UTFit group, on the hand, uses a Bayesian statistical analysis of the measurements and finds $\phi_3 = (68.3 \pm 7.5)°$ compared with their CKM fit $\phi_3 = (69.5 \pm 3.9)°$.

3. Future
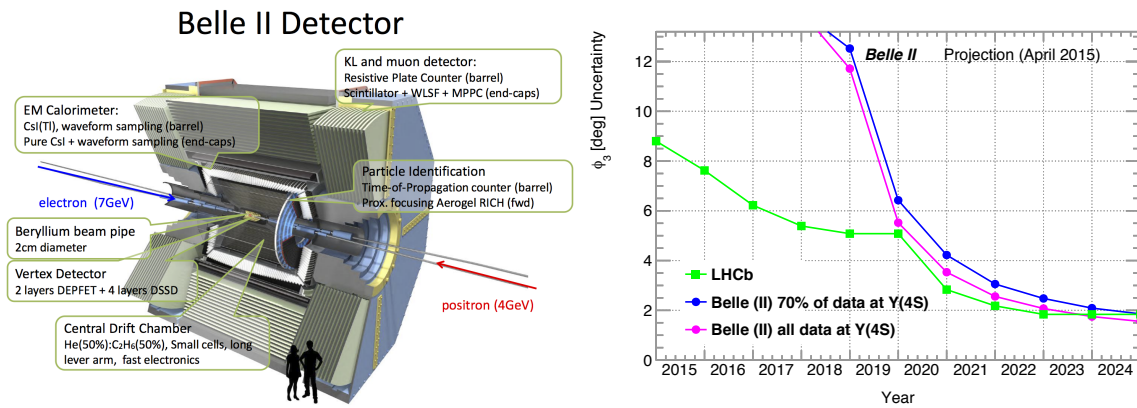
Figure 14: The Belle 2 detector (left) and projections for the future uncertainty on ϕ_3 comparing the Belle 2 and LHCb collaborations. Note that these projections use old expectations for the data collection period for Belle II.

Belle II is targeting high-luminosity and aims to collect 50 ab^{-1} by 2024 [27]. Improved tracking should increase K_S efficiency, improved PID will be available, leading to better K and π separation, and waveform sampling in the calorimeters, improving γ/π^0 reconstruction and therefore leading to better D^{*0} reconstruction. Figure 14 shows the Belle 2 detector and the projections on

the uncertainty of ϕ_3. LHCb is expected to continue their impressive reduction of the uncertainty, and will further upgrade their detector during the long shutdown 2 of the LHC and to commence operation in 2019 [28]. Belle II should reach an equivalent uncertainty to LHCb around 2020. The ultimate precision of 1–2° achievable with the current techniques should be reached by 2025. Ultimately, the precision is limited by irreducible systematic uncertainties, such as the precision of the c_i and s_i inputs from CLEO or BES-III when performing the model-independent GGSZ analysis.

4. Conclusion

The prospects for future ϕ_3 measurements are good. There has been a lot of activity trying to further reduce the already rapidly falling uncertainty in recent years. LHCb is taking more data and exploring new modes, while Belle II will start to be competitive within the next few years. Degree-level precision is on the horizon.

References

[1] N. Cabibbo, "Unitary Symmetry and Leptonic Decays," Phys. Rev. Lett. **10**, 531 (1963).

[2] M. Kobayashi and T. Maskawa, "*CP* Violation in the Renormalizable Theory of Weak Interaction," Prog. Theor. Phys. **49**, 652 (1973).

[3] A. Abashian *et al.* [Belle Collaboration], "The Belle Detector," Nucl. Instrum. Meth. A **479**, 117 (2002).

[4] B. Aubert *et al.* [BaBar Collaboration], "The BaBar detector," Nucl. Instrum. Meth. A **479**, 1 (2002) doi:10.1016/S0168-9002(01)02012-5 [hep-ex/0105044].

[5] A. A. Alves, Jr. *et al.* [LHCb Collaboration], "The LHCb Detector at the LHC," JINST **3**, S08005 (2008).

[6] M. Gronau and D. London, "How to determine all the angles of the unitarity triangle from $B_d^0 \to DK_s$ and $B_s^0 \to D^0\phi$," Phys. Lett. B **253**, 483 (1991).

[7] M. Gronau and D. Wyler, "On determining a weak phase from *CP* asymmetries in charged *B* decays," Phys. Lett. B **265**, 172 (1991).

[8] R. Aaij *et al.* [LHCb Collaboration], "Measurement of *CP* observables in $B^\pm \to DK^\pm$ and $B^\pm \to D\pi^\pm$ with two- and four-body *D* decays," Phys. Lett. B **760**, 117 (2016) [hep-ex/1603.08993].

[9] Y. Amhis *et al.*, "Averages of b-hadron, c-hadron, and tau-lepton properties as of summer 2014," [hep-ex/1412.7515] and online update at http://www.slac.stanford.edu/xorg/hfag

[10] D. Atwood, I. Dunietz and A. Soni, "Enhanced *CP* Violation with $B \to \mathrm{K}D^0(\overline{D}^0)$ Modes and Extraction of the Cabibbo-Kobayashi-Maskawa Angle γ," Phys. Rev. Lett. **78**, 3257 (1997)

[11] D. Atwood, I. Dunietz and A. Soni, "Improved methods for observing *CP* violation in $B^\pm \to KD$ and measuring the CKM phase γ," Phys. Rev. D **63**, 036005 (2001)

[12] S. Malde *et al.*, "First determination of the *CP* content of $D \to \pi^+\pi^-\pi^+\pi^-$ and updated determination of the *CP* contents of $D \to \pi^+\pi^-\pi^0$ and $D \to K^+K^-\pi^0$," Phys. Lett. B **747**, 9 (2015) [arXiv:1504.05878 [hep-ex]].

[13] T. Evans, S. Harnew, J. Libby, S. Malde, J. Rademacker and G. Wilkinson, "Improved determination of the $D \to K^-\pi^+\pi^+\pi^-$ coherence factor and associated hadronic parameters from a combination of $e^+e^- \to \psi(3770) \to c\bar{c}$ and $pp \to c\bar{c}X$ data," Phys. Lett. B **757**, 520 (2016) [hep-ex/1602.07430].

[14] A. Poluektov *et al.* [Belle Collaboration], "Measurement of ϕ_3 with Dalitz plot analysis of $B^+ \to D^{(*)}K^{(*)+}$ decay," Phys. Rev. D **73**, 112009 (2006) [hep-ex/0604054].

[15] A. Poluektov *et al.* [Belle Collaboration], "Evidence for direct *CP* violation in the decay $B \to D^{(*)}K, D \to K_S\pi^+\pi^-$ and measurement of the CKM phase ϕ_3," Phys. Rev. D **81**, 112002 (2010) [hep-ex/1003.3360].

[16] K. Negishi *et al.* [Belle Collaboration], "First model-independent Dalitz analysis of $B^0 \to DK^{*0}$, $D \to K_S^0\pi^+\pi^-$ decay," PTEP **2016**, no. 4, 043C01 (2016) [arXiv:1509.01098 [hep-ex]].

[17] R. Aaij *et al.* [LHCb Collaboration], "Model-independent measurement of the CKM angle γ using $B^0 \to DK^{*0}$ decays with $D \to K_S^0\pi^+\pi^-$ and $K_S^0K^+K^-$," JHEP **1606**, 131 (2016) [arXiv:1604.01525 [hep-ex]].

[18] A. Giri, Y. Grossman, A. Soffer and J. Zupan, "Determining γ using $B^\pm \to DK^\pm$ with multibody D decays," Phys. Rev. D **68**, 054018 (2003) [hep-ph/0303187].

[19] A. Bondar and A. Poluektov, "The use of quantum-correlated D^0 decays for ϕ_3 measurement," Eur. Phys. J. C **55**, 51 (2008) [arXiv:0801.0840 [hep-ex]].

[20] J. Libby *et al.* [CLEO Collaboration], "Model-independent determination of the strong-phase difference between D^0 and $\bar{D}^0 \to K_{S,L}^0 h^+h^-$ ($h = \pi, K$) and its impact on the measurement of the CKM angle γ/ϕ_3," Phys. Rev. D **82**, 112006 (2010) [arXiv:1010.2817 [hep-ex]].

[21] H. Aihara *et al.* [Belle Collaboration], "First Measurement of ϕ_3 with a Model-independent Dalitz Plot Analysis of $B \to DK, D \to K_S\pi\pi$ Decay," Phys. Rev. D **85**, 112014 (2012) [arXiv:1204.6561 [hep-ex]].

[22] R. Aaij *et al.* [LHCb Collaboration], "Measurement of the CKM angle γ using $B^\pm \to DK^\pm$ with $D \to K_S^0\pi^+\pi^-, K_S^0K^+K^-$ decays," JHEP **1410**, 097 (2014) [arXiv:1408.2748 [hep-ex]].

[23] R. Aaij *et al.* [LHCb Collaboration], "Constraints on the unitarity triangle angle γ from Dalitz plot analysis of $B^0 \to DK^+\pi^-$ decays," Phys. Rev. D **93**, no. 11, 112018 (2016) hep-ex/1602.03455.

[24] LHCb Collaboration "Measurement of the CKM angle γ from a combination of $B \to DK$ analyses," LHCb-CONF-2016-001.

[25] J. Charles *et al.* [CKMfitter Group], "*CP* Violation and the CKM Matrix: Assessing the Impact of the Asymmetric *B* Factories," Eur. Phys. J. C41, 1-131 (2005) [hep-ph/0406184], updated results and plots from http://ckmfitter.in2p3.fr

[26] M. Bona *et al.* [UTfit Collaboration], "The Unitarity Triangle Fit in the Standard Model and Hadronic Parameters from Lattice QCD", JHEP 10 (2006) 081 [hep-ph/0606167], updated results and plots from http://www.utfit.org/UTfit/ResultsSummer2014PostMoriond

[27] T. Abe *et al.* [Belle-II Collaboration], "Belle II Technical Design Report," KEK Report 2010-1 [arXiv:1011.0352].

[28] I. Bediaga et al. [LHCb Collaboration], "Framework TDR for the LHCb Upgrade: Technical Design Report," CERN-LHCC-2012-007 (2012).